doi: 10.5028/jatm.v10.924 ORIGINAL PAPER

Effect of Convergent Section Contour on the Sonic Line in Rocket Engine Nozzles

Eduardo Matos Germer[1], Carlos H. Marchi[2]

Germer EM http://orcid.org/0000-0001-7227-2249
Marchi CH http://orcid.org/0000-0002-1195-5377

How to cite

Germer EM; Marchi CH (2018) Effect of Convergent Section Contour on the Sonic Line in Rocket Engine Nozzles. J Aerosp Technol Manag, 10: e3218. doi: 10.5028/jatm.v10.924.

ABSTRACT: This study made a numeric evaluation of the effect of convergent geometry on the position and profile of the sonic line in rocket engine nozzles. To validate the numerical solution, two conical nozzles, from which experimental results are available in the literature, were used as reference. The tested convergent geometries have the same values for throat radius (R_t), radius of curvature at the throat of the divergent section (R_{c3}), divergent length, and ratio of areas. The numerical solutions have shown that convergent geometry changes the shape of the sonic line, and nozzles with lower radius ratios (R_{c2}/R_t) are more sensitive to the shape of the convergent section.

KEYWORDS: Nozzle, Sonic line, Convergent, Rocket engine, Propulsion, Validation.

INTRODUCTION

Nozzle design should take into account the optimization of performance parameters, such as thrust, while producing nozzles with the smallest mass possible, so that there is little impact on the total load of launch vehicles. One way to reach this goal is to shorten nozzle length. This leads to the construction of nozzles with low radii of curvature (R_{c2}), and consequently low radius ratios (R_{c2}/R_t) in the convergent/throat transition (Fig. 1).

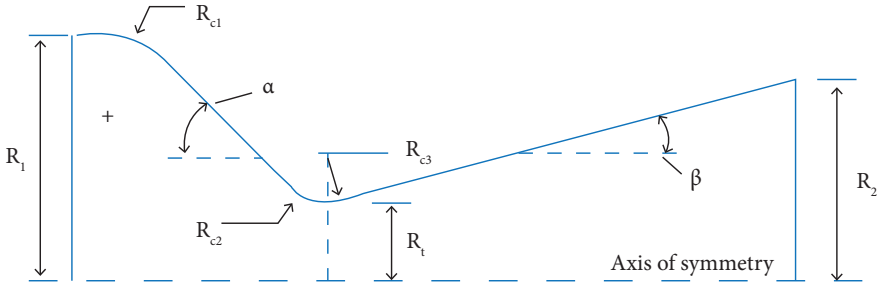

Figure 1. Geometric characteristics of a nozzle.

The method of characteristics is widely used in nozzle design projects. One of the premises for using this method is to learn about the position/shape of the sonic line. Some series have been used to gather this information. While they are effective for ratios $R_{c2}/R_t > 1$, they are not as suitable for $R_{c2}/R_t < 1$ (Wear 1971).

1.Universidade Tecnológica Federal do Paraná – Departamento Acadêmico de Mecânica – Curitiba/PR – Brazil.
2.Universidade Federal do Paraná – Departamento de Engenharia Mecânica – Laboratório de Experimentação Numérica – Curitiba/PR – Brazil.
Correspondence author: Eduardo Matos Germer | Universidade Tecnológica Federal do Paraná – Departamento Acadêmico de Mecânica) | Rua Deputado Heitor Alencar Furtado, 5000 | CEP: 81.280-340 – Curitiba/PR – Brazil | E-mail: eduardomg@utfpr.edu.br
Received: May 23, 2017 | **Accepted:** Aug. 8, 2017
Section Editor: Fernando Costa

Figure 1 shows the main geometric characteristics of a conical nozzle: radius of the nozzle inlet (R_1); radius of curvature between the combustion chamber and the convergent section (R_{c1}); semi-angle of the cone of the convergent section (α); radius of curvature between the cone of the convergent section and the throat (R_{c2}); radius of curvature between the throat and the cone of the divergent section (R_{c3}); radius of the throat (R_t); semi-angle of the divergent section (β); and radius of the nozzle outlet (R_2).

METHOD

The numerical solution for the flow at convergent-divergent (CD) supersonic nozzles uses the Navier-Stokes equations to represent the flow. Such equations can be simplified by considering a steady state, inviscid fluid, in an axisymmetric nozzle profile, thus resulting in mass, momentum (Euler equations) and energy conservation equations (Eqs. 1 to 4) (Bird *et al.* 2006).

$$\frac{\partial(\rho u)}{\partial x}+\frac{1}{y}\frac{\partial(\rho y v)}{\partial y}=0 \tag{1}$$

$$\frac{\partial(\rho u u)}{\partial x}+\frac{1}{y}\frac{\partial(\rho y v u)}{\partial y}=-\frac{\partial p}{\partial x} \tag{2}$$

$$\frac{\partial(\rho u v)}{\partial x}+\frac{1}{y}\frac{\partial(\rho y v v)}{\partial y}=-\frac{\partial p}{\partial y} \tag{3}$$

$$c_p\left[\frac{\partial(\rho u T)}{\partial x}+\frac{1}{y}\frac{\partial(\rho y v T)}{\partial y}\right]=u\frac{\partial p}{\partial x}+v\frac{\partial p}{\partial y} \tag{4}$$

where: x is axial coordinate; y is radial coordinate; u is velocity component in x; v is velocity component in y; T is absolute temperature; c_p is specific heat at constant pressure; p is pressure; and ρ is density. The fluid is the air, considered to be a thermally perfect and calorically imperfect gas; thus, the equation for closure of the mathematical model is given by the equation of state for a perfect gas (Eq. 5). Considering R as the gas constant,

$$p=\rho R T \tag{5}$$

The model for defining specific heat at constant pressure, considering a calorically imperfect gas, was extracted from NACA (1953) is shown in Eq. 6:

$$c_p=(c_p)_{perf}\left\{1+\frac{\gamma_{perf}-1}{\gamma_{perf}}\left[\left(\frac{\theta}{T}\right)^2\frac{e^{\theta/T}}{\left(e^{\theta/T}-1\right)^2}\right]\right\} \tag{6}$$

where: γ is the ratio of specific heats; θ is a reference temperature; and the sub-index *perf* indicates the values for calorically perfect gas.

The value of the reference temperature (θ) is 3056 K (5500 °R). With this value, the error predicted for the ratio of specific heats is up to 3% for temperature ranges from above that of liquefaction until 2778 K (5000 °R), and pressures up to 2.5 MPa (25 atm). Specific heats at constant pressure and volume for diatomic and calorically perfect gas are 3.5 R and 2.5 R, respectively, and their ratio is 1.4.

Discretization of the physical domain was performed by dividing the nozzles into six segments in *x*, and each one of these was divided into a certain number of uniform volumes of control per segment. The number of volumes in each segment was defined in order to make the mesh practically uniform in *x*. The base mesh was thicker, and its elements in *x* measured approximately 2.54 mm, while the ones in the thinner mesh measured 0.16 mm. In the radial direction, the mesh is uniform per section. This form of discretization does not affect the numerical solution because the flow is inviscid; therefore, the existence of the boundary layer is disregarded.

Figure 2 shows an example of mesh for a conic nozzle with 30° convergent semi-angle (α) and 15° divergent semi-angle (β). As the mesh is structured and non-orthogonal, Eqs. 1 to 4 were transformed into computational space (Maliska 2004). After that, they were discretized using the finite volume method. Although flow was assessed in steady state, the false transient technique was used to facilitate convergence, while temporal discretization was totally implicit.

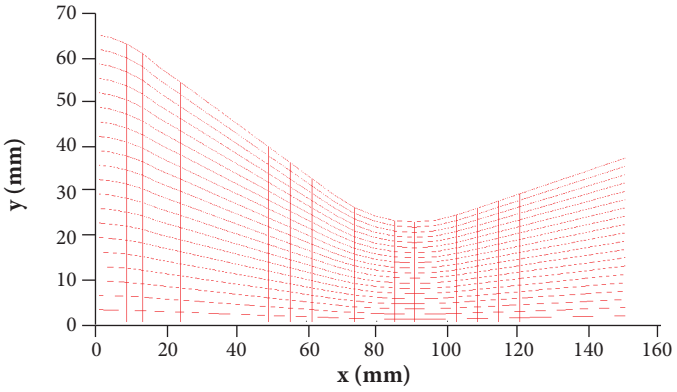

Figure 2. Mesh for 30° – 15° conic nozzle.

Pressures (p_{inlet}) and temperatures (T_{inlet}) at the nozzle inlet are obtained by considering the isentropic flow originating at the combustion chamber. They are functions of stagnation pressure and stagnation temperature, as well as velocity components in this region. The equations can be found in Sutton and Biblarz (2010).

The advective terms were approximated with the upwind scheme (UDS), and the pressure term has been approximated with the central difference scheme (CDS-2). Therefore, theoretically, the order of accuracy of the solution is equal to that of the unit. The arrangement is co-located, i.e., the variables are evaluated at the centers of volumes, whose position is centered in relation to the faces.

To solve the velocity-pressure coupling, the SIMPLEC method was applied to any velocity regimes (Marchi and Maliska 1994). The boundaries are treated with ghost volumes and the boundary conditions are given in Fig. 3. The wall is considered to be adiabatic.

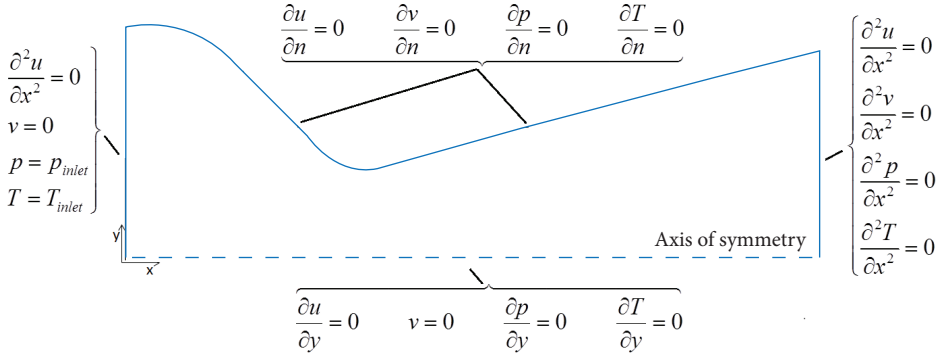

Figure 3. Boundary conditions.

According to ASME (2009), validation is the process that defines the degree of accuracy of a theoretical model when representing a real phenomenon; it is about the comparison between numerical and experimental results. For the proposed numerical solution, the validation was based on some nozzles presented in the work of Back *et al.* (1965). Table 1 shows the values of geometric parameters, already referenced in Fig. 1, of one of these nozzles, with 45° convergent semi-angle (α) and 15° divergent semi-angle (β).

Table 1. Data on nozzle BMG45-15 used in the validation.

R_1 (mm)	R_{c1} (mm)	$R_{c2} = R_{c3}$ (mm)	R_t (mm)	R_{c2}/R_t	R_2 (mm)	Stagnation pressure (MPa)	Stagnation temperature (K)	Mass flow rate (kg/s)
63.5	20.3	12.7	20.3	0.625	52.3	1.73	833	3.04

The validation showed that the numerical modeling represents the phenomenon appropriately. Modeling error for pressure on the nozzle wall can reach 0.4% in the convergent section, 3.0% in the throat region and 3.3% in the divergent section, while mass flow rate had a modeling error of 0.1%.

RESULTS

The assessments below were made on the basis of some nozzles developed from the profile of nozzle BMG45-15. All geometric characteristics of the throat until the outlet of the nozzle were maintained. The semi-angles of the six profiles are different at the conical section of the convergent, and also for the radius ratio (R_{c2}/R_t). Table 2 shows the geometric characteristics that set them apart.

Table 2. Characteristics of the evaluated nozzles.

R_{c2}/R_t	Half angle (α)	
	30°	80°
0.375	Proto 37	Proto 31
0.625	Proto 38	Proto 30
1.0	Proto 39	Proto 32

After defining the nozzles used in the study, numerical simulations were performed, considering the air, under the same conditions of temperature and pressure applied to the validation of the numerical solution (Table 1).

Figures 4a, 4b and 4c show the position/profile of the sonic line for the evaluated nozzles. They show the sonic lines obtained by the numerical solution in each one of the nozzles, and also the position of the sonic line for the case of the quasi-one-dimensional (1D) solution, which coincides with the position of the throat. It can be seen that in nozzles with lower radius ratio (Proto 31 and 37), the effect of the semi-angle of the convergent section is more pronounced than in the nozzles whose radius ratios are greater (Proto 30, 38, 32 and 39).

In Figure 4a, the sonic line of the nozzle whose semi-angle is 80° (Proto 31) has greater curvature than the one with 30° semi-angle (Proto 37), i.e., the sonic line of Proto 31 hits the wall before and the line of symmetry after the sonic line of Proto 37. In a nozzle with low radius ratio, the increase in the slope of the convergent motions the sonic line, on the axis of symmetry, towards the nozzle outlet. This result was observed by Hopkins and Hill (1966). The difference of the result of Hopkins and Hill (1966) is that the authors indicated a small variation in the position of the sonic line on the wall, while the change to the location on the wall is greater than on the axis of symmetry.

Considering the shape of the sonic line given by Fig. 5, Table 3 shows the amplitude of the sonic line on each nozzle. It can be seen that the amplitude (curvature) of the sonic line is higher in nozzles with higher semi-angle of the convergent section. In other words, the slope of the convergent affects the flow pattern at the throat.

Amplitude was defined here as Eq. 7:

$$\text{Amplitude} = x_{symmetry} - x_{wall} \tag{7}$$

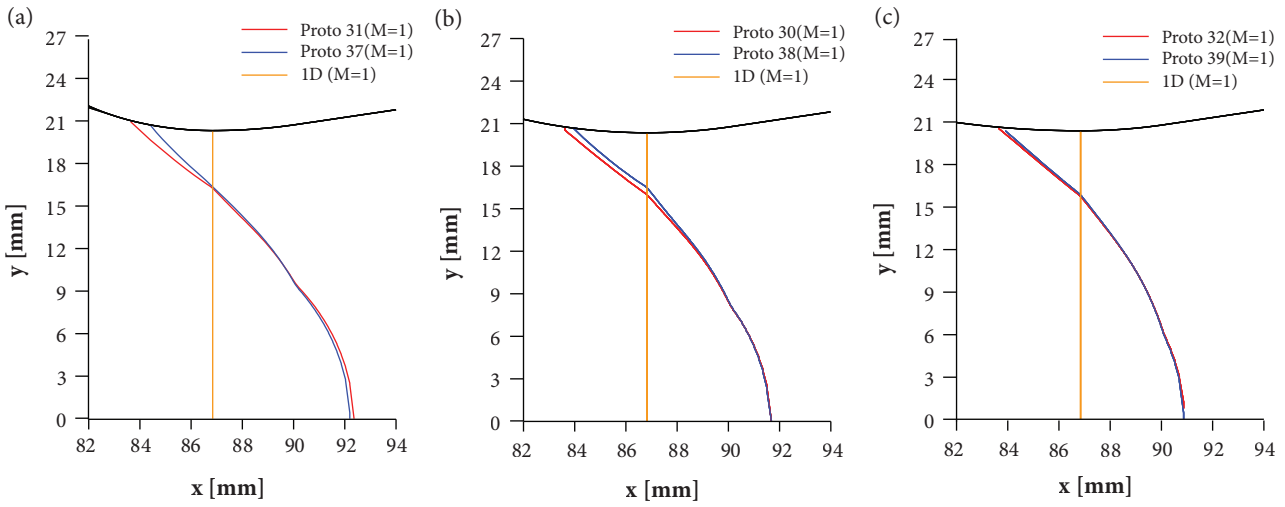

Figure 4. Sonic line (M = 1) for: (a) Proto 31 and Proto 37; (b) Proto 30 and Proto 38; and (c) Proto 32 and Proto 39.

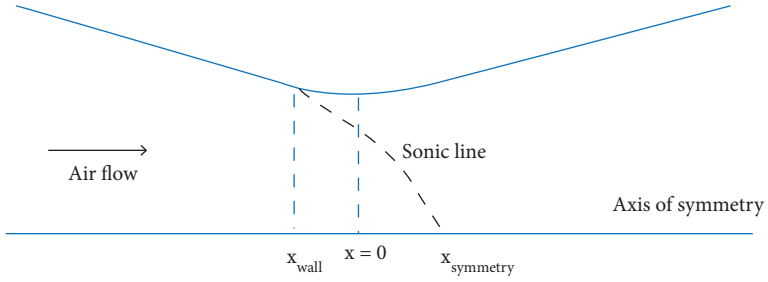

Figure 5. Scheme of the coordinates of the sonic line on the wall and on the axis of symmetry.

Table 3. Position of the sonic line on the wall and on the line of symmetry with x = 0 at the throat.

Nozzle #	R_{c1} (mm)	α (°)	R_{c2} (mm)	R_{c2}/R_t (adim)	x_{wall} (mm)	$x_{simmetry}$ (mm)	Amplitude (mm)
Proto 31	20.3	80	7.6	0.375	–3.25	5.47	8.72
Proto 37	20.3	30	7.6	0.375	–2.49	5.30	7.79
Proto 30	20.3	80	12.7	0.625	–3.41	4.80	8.21
Proto 38	20.3	30	12.7	0.625	–2.93	4.80	7.73
Proto 32	20.3	80	20.3	1	–3.25	4.14	7.39
Proto 39	20.3	30	20.3	1	–3.15	3.97	7.12

Figure 6 shows the Mach number curves at the outlet of the nozzles, both on the line of symmetry and on the wall, as well as the values of the quasi-one-dimensional (1D) solution. Figure 6a shows the nozzles whose radius ratio is 0.375; Fig. 6b, those whose radius ratio is 0.625; and Fig. 6c, the ones with radius ratio of 1.0. In each of the figures, the semi-angle of the convergent section of the first nozzle is 80° (Proto 30, 31 and 32) and that of the second nozzle, 30° (Proto 37, 38, 39).

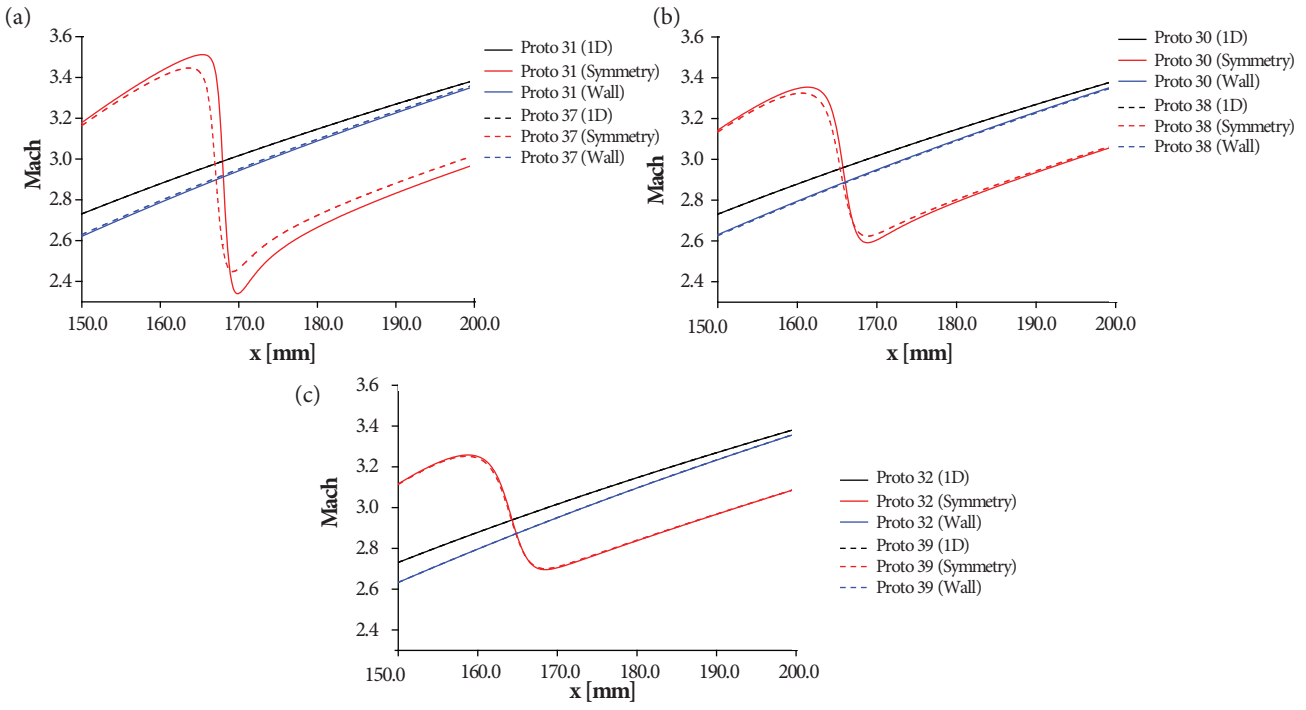

Figure 6. Values of the Mach number on the axis of symmetry and on the wall, and the quasi-one-dimensional solution at the outlet of the nozzles for: (a) Proto 31 and Proto 37; (b) Proto 30 and Proto 38; and (c) Proto 32 and Proto 39.

The variation in the Mach number on the axis of symmetry, as shown in Figs. 6a, 6b and 6c, is due to the oblique shock wave that appears on the wall, at the point of transition between the curve of the throat and the cone of the divergent section, and it spreads until it reaches the axis of symmetry. Figure 6a shows that the nozzle with semi-angle of 30° (Proto 37) has a less intense shock wave along the axis of symmetry than the nozzle with semi-angle of 80° (Proto 31). The lesser intensity corresponds to the lower reduction of the Mach number of the flow while passing through the shock wave. The result of such less intense internal shock wave in Proto 37 is a higher Mach number on the axis of symmetry at the nozzle outlet. As the Mach values for Proto 31 and Proto 37 on the wall and at the nozzle outlet are very similar, it suggests that the Mach field of Proto 37, in the outlet section, is larger than that of nozzle Proto 31. As a result, the thrust coefficient of nozzle Proto 37 is 0.61% greater than that of Proto 31. This behavior is also shown in Figs. 6b and 6c, but with less intensity. In Fig. 6c, the difference in Mach between the two nozzles on the axis of symmetry, at the nozzle outlet, is almost imperceptible.

This impact of the radius of curvature (R_{c2}) on shock wave intensity had already been identified by Pirumov *et al.* (1974). According to the authors, this shock wave begins at the point of transition from the curvature of the throat and the divergent section, thus generating a compression wave that results in a shock wave, increasing in intensity as it approaches the axis of symmetry. As it reflects on the axis of symmetry of this wave, it decreases in intensity. The authors suggest that shock wave intensity increases as the radius of curvature (R_{c2}) is decreased, a behavior that was confirmed by comparing nozzles Proto 31 and 37 (Fig. 6a), and nozzles Proto 32 and 39 (Fig. 6c), which have greater radius of curvature.

CONCLUSION

The main objective of the present study was to evaluate the effect of contour of the convergent section of conical nozzles on the sonic line. It was found that the semi-angle of the convergent section (α) and the R_{c2}/R_t ratio affect the position and shape of the sonic line as well as the flow at the nozzle outlet. Nozzles with high $R_{c2}/R_t \geq 1$ ratios are hardly influenced by convergent

section contour, while nozzles with small radius ratios ($R_{c2}/R_t < 1$) are influenced by convergent section contour. Some of these results are in agreement with studies published in the literature.

AUTHOR'S CONTRIBUTION

Conceptualization, Germer E and Marchi CH; Methodology, Germer E and Marchi CH; Investigation, Germer E; Writing – Original Draft, Germer E; Writing – Review and Editing, Marchi CH; Resources, Germer E and Marchi CH; Supervision, Marchi CH.

ACKNOWLEDGEMENTS

The authors would like to acknowledge the financial support provided by CNPq (Conselho Nacional de Desenvolvimento Científico e Tecnológico - Brazil), AEB (Agência Espacial Brasileira – Brazil) by the Uniespaço Program, and CAPES (Coordenação de Aperfeiçoamento de Pessoal de Nível Superior - Brazil). The second author is supported by a CNPq scholarship.

REFERENCES

ASME V&V (2009) Standard for verification and validation in computational fluid dynamics and heat transfer. Washington: ASME.

Back LH, Massier PF, Gier HL (1965) Comparison of measured and predicted flows through conical supersonic nozzles with emphasis on transonic region. AIAA Journal 3(9):1606-1614.

Bird RB, Stewart WE, Lightfoot EN (2006) Transport Phenomena. 2nd ed. New York: John Wiley & Sons.

Hopkins DF, Hill DE (1966) Effect of small radius of curvature on transonic flow in axisymmetric nozzles. AIAA Journal 4(8):1337-1343. doi: 10.2514/3.3674

Maliska CR (2004) Transferência de calor e mecânica dos fluidos computacional. 2nd ed. Rio de Janeiro: LTC.

Marchi CH, Maliska CR (1994) A nonorthogonal finite-volume method for the solution of all speed flows using co-located variables. Numerical Heat Transfer, Part B 26(3):293-311. doi: 10.1080/10407799408914931

NACA (1953) Equations, Table and Charts for Compressible Flow. (NACA-TR-1135) NACA Technical Report.

Pirumov UG, Roslyakov GS, Sukhorukov VP (1974) Investigation of supersonic flows in conical nozzles. Fluid Dynamics 9(3):415-420. doi: 10.1007/BF01025525

Sutton GP, Biblarz O (2010) Rocket propulsion elements. 8th ed. New York: John Wiley & Sons.

Wear RR (1971) Numerical computation of transonic flow in nozzles with small throat radii of curvature (Retrospective Theses and Dissertations, 4519). Ames: Iowa State University.